ARTICLE   OPEN

High-energy magnetic excitations from heavy quasiparticles in CeCu₂Si₂

Yu Song [1,2,3,4 ✉], Weiyi Wang[1], Chongde Cao [5 ✉], Zahra Yamani[6], Yuanji Xu[7,8], Yutao Sheng[7,8], Wolfgang Löser[9], Yiming Qiu [10], Yi-feng Yang [7,8,11], Robert J. Birgeneau[2,3] and Pengcheng Dai [1 ✉]

Magnetic fluctuations is the leading candidate for pairing in cuprate, iron-based, and heavy fermion superconductors. This view is challenged by the recent discovery of nodeless superconductivity in CeCu₂Si₂, and calls for a detailed understanding of the corresponding magnetic fluctuations. Here, we mapped out the magnetic excitations in superconducting (S-type) CeCu₂Si₂ using inelastic neutron scattering, finding a strongly asymmetric dispersion for $E \lesssim 1.5$ meV, which at higher energies evolves into broad columnar magnetic excitations that extend to $E \gtrsim 5$ meV. While low-energy magnetic excitations exhibit marked three-dimensional characteristics, the high-energy magnetic excitations in CeCu₂Si₂ are almost two-dimensional, reminiscent of paramagnons found in cuprate and iron-based superconductors. By comparing our experimental findings with calculations in the random-phase approximation, we find that the magnetic excitations in CeCu₂Si₂ arise from quasiparticles associated with its heavy electron band, which are also responsible for superconductivity. Our results provide a basis for understanding magnetism and superconductivity in CeCu₂Si₂, and demonstrate the utility of neutron scattering in probing band renormalization in heavy fermion metals.

INTRODUCTION

The discovery of superconductivity in CeCu₂Si₂[1] marked the beginning of decades-long intense research into unconventional superconductivity[2,3], encompassing cuprate[4–6], iron-based[7–10], and heavy fermion superconductors[11–13]. The proximity of superconductivity to antiferromagnetic (AF) quantum critical points (QCP) in these systems implicate AF fluctuations that proliferate at the AF QCP as the pairing glue, leading to unconventional superconductivity with a sign-changing superconducting order parameter[2,3,14].

Experimental evidence for magnetically driven superconductivity in these systems include: (i) reduction of the magnetic exchange energy is much larger than the superconducting condensation energy[15–22]; (ii) the observation of a spin resonance mode, which in the spin-exciton scenario indicates a sign-changing superconducting order parameter[2,23–25]; and (iii) the persistence of two-dimensional (2D) high-energy AF fluctuations that resemble spin waves in magnetically ordered parent compounds[19,26–33].

From an empirical perspective, it is important to identify whether these features are common in different unconventional superconductors, so that ingredients for a unified pairing mechanism may be established. Of the above observations, (i) is model-independent and has been verified for cuprate, iron-based and heavy fermion superconductors[15–22]; (ii) the spin resonance mode has been found in cuprate, iron-based, and heavy fermion superconductors, but their spin-excitonic nature needs to be separately tested and requires a quasiparticle origin of the magnetic excitations[2,23,24]; while (iii) has been established for

cuprate and iron-based superconductors[19,26–33], magnetic excitations in heavy fermion superconductors such as CeCu₂Si₂ are strongly three-dimensional (3D) at low energies[18], and it is unclear whether they become 2D at higher energies.

CeCu₂Si₂ (S-type) is an archetypal heavy fermion unconventional superconductor, and is naturally located near a 3D AF QCP[34,35]. Upon the introduction of slight Cu deficiencies the system can be tuned to AF order (A-type), with an ordering vector $\tau \approx (0.22, 0.22, 0.53)$ [Fig. 1a][36]. Similar dispersive paramagnons up to $E \approx 1$ meV were found to stem from τ in both A-type and S-type CeCu₂Si₂[18,37]. While these dispersive AF fluctuations were discussed in terms of an effective Heisenberg model with short-range magnetic couplings[18], magnetic order in A-type CeCu₂Si₂ was suggested to result from Fermi surface nesting[36], and AF fluctuations in CeCu₂Si₂ were found to exhibit critical slowing down consistent with being near a spin-density-wave QCP[35]. In the superconducting state of CeCu₂Si₂, a spin gap forms with spectral weight built up just above it[18], consistent with the formation of a spin resonance mode with an energy $E_r \approx 0.2$ meV, which in the spin-excitonic scenario suggests magnetic pairing[38,39]. The recent discovery of fully-gapped superconductivity in CeCu₂Si₂[40–48] challenges the role of magnetic excitations in its superconducting state and calls for a more detailed understanding of its magnetism, including the origin and high-energy properties of its magnetic excitations.

In this work, by carrying out detailed inelastic neutron scattering measurements over large energy and momentum ranges, we uncover magnetic fluctuations up to $E \gtrsim 5$ meV in CeCu₂Si₂. While magnetic fluctuations below $E \approx 1.5$ meV are strongly 3D and dispersive[18,35], they become increasingly 2D with

¹Department of Physics and Astronomy, Rice University, Houston, TX, USA. ²Department of Physics, University of California, Berkeley, CA, USA. ³Materials Sciences Division, Lawrence Berkeley National Laboratory, Berkeley, CA, USA. ⁴Center for Correlated Matter and Department of Physics, Zhejiang University, Hangzhou, China. ⁵MOE Key Laboratory of Materials Physics and Chemistry under Extraordinary Conditions and Shaanxi Key Laboratory of Condensed Matter Structures and Properties, School of Physical Science and Technology, Northwestern Polytechnical University, Xian, China. ⁶National Research Council, Chalk River, Ontario, Canada. ⁷Beijing National Laboratory for Condensed Matter Physics and Institute of Physics, Chinese Academy of Sciences, Beijing, China. ⁸University of Chinese Academy of Sciences, Beijing, China. ⁹Leibniz-Institut für Festkörper- und Werkstoffforschung (IFW) Dresden, Dresden, Germany. ¹⁰NIST Center for Neutron Research, National Institute of Standards and Technology, Gaithersburg, MD, USA. ¹¹Songshan Lake Materials Laboratory, Dongguan, Guangdong, China. ✉email: yusong_phys@zju.edu.cn; caocd@nwpu.edu.cn; pdai@rice.edu
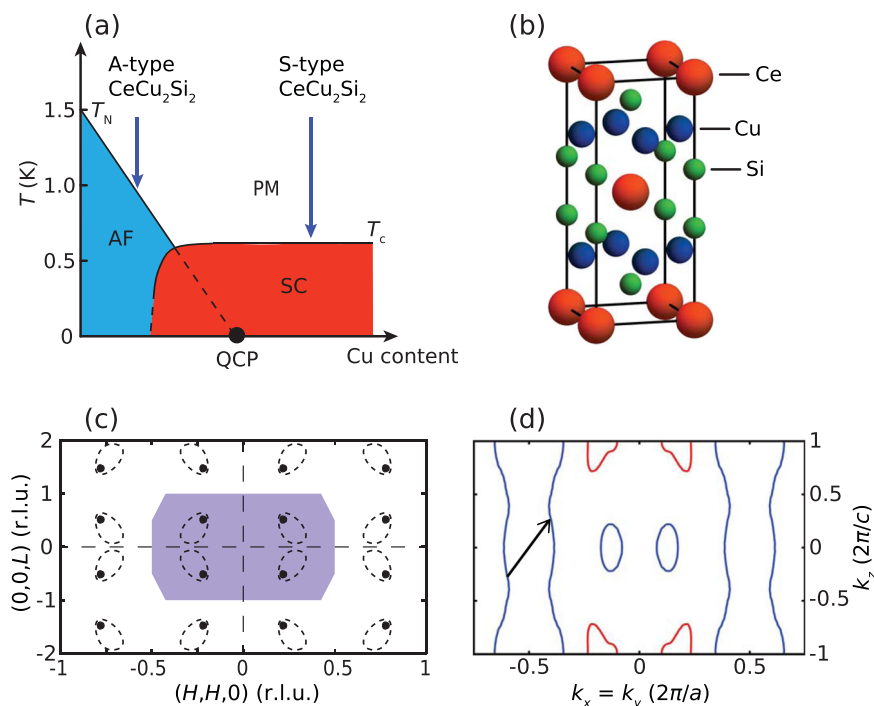
Fig. 1 Crystal structure, phase diagram, and reciprocal space of CeCu$_2$Si$_2$. a Schematic phase diagram of CeCu$_2$Si$_2$. **b** Crystal structure of CeCu$_2$Si$_2$, with Ce^{3+} ions forming a body-centered tetragonal lattice. **c** $[H, H, L]$ scattering plane of CeCu$_2$Si$_2$, with the shaded area representing a Brillouin zone for the Ce^{3+} ions. The black dots indicate magnetic Bragg peaks in A-type CeCu$_2$Si$_2$[36], and the dashed ovals are schematic intensity contours of low-energy AF excitations in our S-type CeCu$_2$Si$_2$. **d** Slice of the CeCu$_2$Si$_2$ Fermi surface with $k_x = k_y$, and the arrow represents the intraband nesting vector. The electronic structure used in this work is identical to that in ref. [46], and 3D plots of the Fermi surfaces are shown in Supplementary Fig. 7.

increasing energy and form an almost dispersionless column in energy. By comparing with theoretical calculations, we find magnetic excitations in CeCu$_2$Si$_2$ can be accounted for by intraband scattering of quasiparticles associated with the heavy electron band [Fig. 1d], and therefore allowing us to estimate the band renormalization by matching our calculations with experimental data. We expect this method to be broadly applicable in heavy fermion metals near magnetic criticality. The agreement between our experimental and theoretical results suggests that despite signatures of non-Fermi-liquid behavior[34,35], the magnetic excitations in the normal state of CeCu$_2$Si$_2$ are reasonably captured by a LDA+U band structure with additional mass renormalization. Our discovery of almost 2D high-energy magnetic excitations in CeCu$_2$Si$_2$ is reminiscent of similar findings in cuprate and iron-based superconductors, and favors magnetic pairing with a sign-changing superconducting order parameter.

RESULTS

Inelastic neutron scattering

Large single crystals of S-type CeCu$_2$Si$_2$ with $T_c \approx 0.5$ K were grown using a vertical floating zone method[49]. Multiple crystals with a total mass of ≈12 g were co-aligned in the $[H, H, L]$ scattering plane using the E3 four-circle neutron diffractometer at the Chalk River Laboratory (see Methods for details). Inelastic neutron scattering measurements were carried out using the Multi-Axis Crystal Spectrometer (MACS)[50] at the NIST Center for Neutron Research, with fixed outgoing neutron energies $E_f = 3$ or 5 meV. We reference momentum transfer $\mathbf{Q} = (H, K, L)$ in reciprocal lattice units, with $H = aQ_x/(2\pi)$, $K = bQ_y/(2\pi)$, and $L = cQ_z/(2\pi)$ ($a = b \approx$ 4.1 Å and $c \approx 9.9$ Å). Ce^{3+} ions in CeCu$_2$Si$_2$ form a body-centered tetragonal lattice [Fig. 1b], and the corresponding Brillouin zone in the $[H, H, L]$ plane is shown in Fig. 1c. Isotropic background

intensities were estimated from regions with $H = 0$ and 1, and have been subtracted from our data.

Maps of the $[H, H, L]$ plane at $T = 1.6$ K are compared in the left column of Fig. 2 for different energies, with the corresponding cuts along $(H, H, 1.48)$ and $(0.22, 0.22, L)$ shown in the middle and right columns. For $E = 0.5$ meV, magnetic excitations are relatively sharp, with spectral weight asymmetrically located around τ [Figs. 1c, 2a–c]. With increasing energy, the magnetic excitations gradually broaden, while maintaining the asymmetric distribution of spectral weight around τ [Fig. 2d–o]. Given the same asymmetric distribution is observed for multiple momentum and energy transfers, it is an intrinsic effect rather than a result of instrumental resolution. Two dispersive branches were previously observed at low energies in CeCu$_2$Si$_2$[18], with the branch closer to the zone boundary being increasingly dominant in intensity with increasing energy[18]. In our results, a single branch is resolved and can be identified as the dominant branch in previous work, while the weaker branch is unresolved and likely shows up as a shoulder in intensity. Clear modulation of magnetic intensity along $(H, H, 1.48)$ persists up to the highest measured energy ($E = 5.5$ meV), with little or no magnetic intensity at the $(0, 0, L)$ and $(1, 1, L)$ positions; on the other hand, intensity along $(0.22, 0.22, L)$ becomes weakly L-dependent for $E \geq 2$ meV. These observations suggest that although CeCu$_2$Si$_2$ is close to a 3D AF QCP[34,35], its high-energy magnetic excitations are almost 2D (see Supplementary Note 1 and Supplementary Fig. 1 for theoretical evidence of quasi-2D magnetic excitations), similar to cuprate and iron-based superconductors.

Dispersion of the magnetic excitations can be directly visualized in the energy-$(H, H, 1.48)$ map in Fig. 3a. By fitting scans along $(H, H, 1.48)$ using Gaussian peaks symmetrically positioned around $(0.5, 0.5, 1.48)$ as shown in the middle column of Fig. 2, the magnetic dispersion along $(H, H, 1.48)$ can be quantitatively extracted from $E = 0.5$ meV to 5.5 meV [Fig. 3a] (see Methods
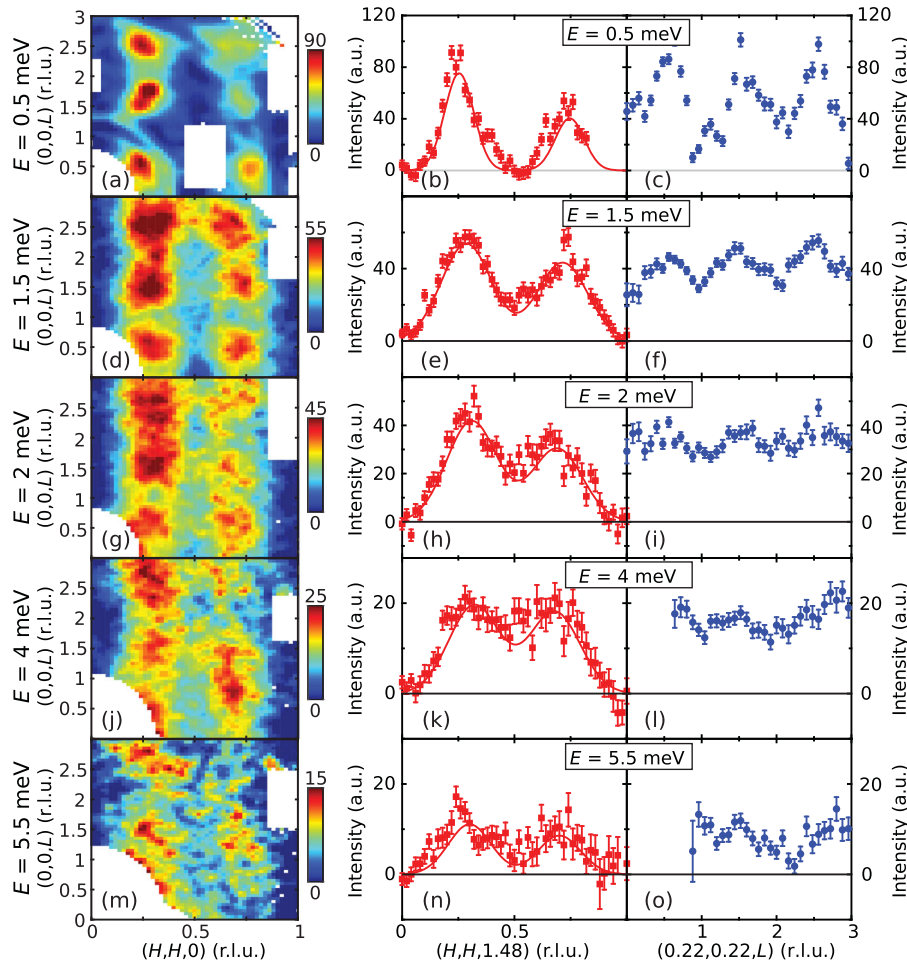
Fig. 2 Wave vector dependence of spin excitations in CeCu$_2$Si$_2$ as a function of energy. Constant-energy maps of the [H, H, L] plane for different energies are shown in the left panels, corresponding cuts along the [H, H, 1.48] direction obtained by binning data with $1.38 < L <$ 1.58 are shown in the middle panels, and corresponding cuts along the [0.22, 0.22, L] direction obtained by binning data with $(0.17, 0.17) < (H, H) < (0.27, 0.27)$ are shown in the right panels. Data in this figure were measured using $E_f = 5$ meV. All vertical error bars represent statistical errors of 1 s.d.

section for details). Consistent with previous observations[18,35,37], the magnetic excitations are dispersive for $E \lesssim 1.5$ meV, but at higher energies they form a column in energy away from the zone boundary. Such an evolution from dispersive to columnar magnetic excitations is unexpected for a local-moment magnetic system, but has been observed in itinerant magnetic systems, including heavily hole-doped iron pnictides[51], Fe-doped MnSi$_3$[52], and MnSi[53].

Theoretical calculations

To understand the origin of the magnetic excitations in CeCu$_2$Si$_2$ which extend up to at least $E = 5.5$ meV, we calculated magnetic excitations within the random-phase approximation (RPA) [Fig. 3b] using a LDA+U band structure (see Methods for details). As can be seen in Fig. 3b, despite extending over a larger energy scale, the calculated magnetic excitations are in good agreement with our experimental results, with the extracted dispersion consisting of a dispersive part at low energies and a columnar part at high energies (see Methods for details). By introducing an overall band renormalization factor r that scales our LDA+U band structure, excellent agreement between experimental and theoretical dispersions can be achieved [Fig. 3c]. We fit the dispersions with a linear-dispersing part that intersects a columnar part at E_{cross}, with the experimental dispersion further constrained to stem from $\tau = (0.22, 0.22, 0.53)$. Scaling the theoretical dispersion so that

E_{cross} is identical for theoretical and experimental dispersions leads to $r \approx 40$. For comparison, the normal state-specific heat coefficient from our LDA+U band structure is $C/T \approx 50$ mJ/mol K^2, which requires $r \approx 20$ to match the experimental normal state value of ≈ 1.0 J/mol K^2 for $T \to 0$ K[35].

The Ce f electrons in CeCu$_2$Si$_2$ participate in the formation of an electron and a hole Fermi sheet, both indispensable for its superconducting state[46]. Compared to specific heat measurements which contain contributions from all Fermi sheets, magnetic excitations measured by neutron scattering are sensitive to bands that exhibit good nesting properties. Therefore, the larger value of r inferred from our neutron scattering results suggests a larger renormalization factor for the well-nested heavy electron band, relative to the hole band. Such band-dependent renormalization effects have been discussed in the context of iron-based superconductors[54–56], with bands exhibiting markedly different renormalization factors for different Fe 3d orbitals. In addition, while specific heat measurements are only sensitive to states within $\sim k_B T$ (~ 0.1 meV for $T = 1.6$ K) of the Fermi level, magnetic fluctuations probed in our experiments involve states on the order of several meVs within the Fermi level. Therefore, stronger renormalization effects compared to our LDA+U calculations for states away from the Fermi level (relative to those within $k_B T$ of the Fermi level) can also contribute to the larger r values extracted from our inelastic neutron scattering measurements.
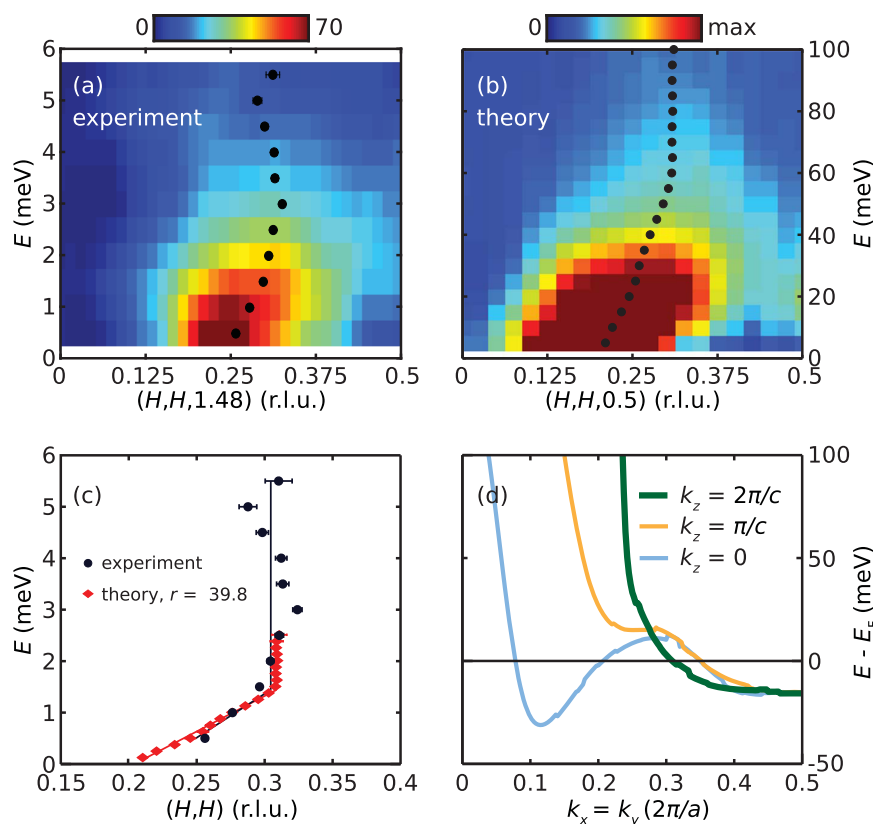
Fig. 3 Dispersion of magnetic excitations in CeCu₂Si₂. a Energy-[H, H, 1.48] map at $T = 1.6$ K obtained by binning data with $1.38 < L < 1.58$. **b** Theoretical energy-[H, H, 0.5] maps obtained from RPA calculations using our LDA+U band structure. **c** Comparison of experimental and theoretical dispersions, with the theoretical dispersion scaled down by the band renormalization factor r. **d** Dispersion of electron-like bands along the $[k_x, k_y = k_x, k_z]$ direction. Data in this figure were measured using $E = 5$ meV. All horizontal error bars are least-square fit errors of 1 s.d.

Our findings illustrate the utility of neutron scattering measurements in extracting renormalization factors with band-specificity, complementing specific heat measurements. It should be noted that such a band-specificity is limited to the well-nested band, which dominates the magnetic excitation spectra, while other bands are effectively not probed. This method hinges on the fact that magnetic excitations arising from quasiparticles encode information on the band structure[57–59], and can be especially useful in heavy fermion metals, for which angle-resolved photoemission spectroscopy measurements are challenging due to the small energy scales involved.

The structure of the heavy electron band along the $(k_x, k_y = k_x, 2\pi/c)$ direction [Fig. 3d] offers an intuitive understanding of the unusual magnetic dispersion in CeCu₂Si₂ [Fig. 3a, b]. The excellent agreement between our experiment and calculations demonstrates that the AF fluctuations in CeCu₂Si₂ are well-described as particle-hole excitations, in which quasiparticles below the Fermi level are excited to unoccupied states above the Fermi level. In our LDA+U calculations (without the renormalization by r), the band bottom is around -15 meV. Therefore, the crossover from dispersive to columnar behavior that occurs at around 60 meV is dominated by states above the Fermi level. Comparing states just above the Fermi level ($E \lesssim 30$ meV) with those well above the Fermi level ($E > 50$ meV) reveals that the latter are much lighter, characteristic of conduction bands from none-f orbitals [Fig. 3d]. Therefore, the crossover from dispersive excitations at low-energies to columnar excitations at high-energies in CeCu₂Si₂ reflects the electron band's reduction of f-orbital content above the Fermi level (see Supplementary Fig. 2 for the partial density states of CeCu₂Si₂ from our LDA+U calculations). For other values of k_z, the band experiences a similar loss of f-orbital content for

$E > 50$ meV, although more complex behaviors are seen closer to the Fermi level.

Temperature evolution of low-energy magnetic excitations

Maps of the $[H, H, L]$ plane for $E = 0.3$ meV at $T = 0.3$ K ($T < T_c$) and 1.6 K ($T > T_c$) are compared in Fig. 4a, b, with their difference shown in Fig. 4c. Since $E = 0.3$ meV is above the energy window of the spin resonance mode in CeCu₂Si₂ ($E_r \approx 0.2$ meV)[18], magnetic excitations in the superconducting and normal states are similar. Examining the difference of excitations measured at $T = 0.3$ K and 1.6 K nonetheless reveals a subtle shift of magnetic spectral weight toward the Brillouin zone center along the (H, H) direction upon cooling. The systematic presence of such behavior across multiple Brillouin zones [Fig. 4c] demonstrates this behavior to be an intrinsic property of CeCu₂Si₂. Cuts along the $(H, H, 1.5)$ direction are compared in Fig. 4d for $T = 0.3$ and 1.6 K, and their difference is shown in Fig. 4e. Such a temperature-dependent shift is similar to the shift of ordering vector[36] and magnetic excitations[35] in A-type CeCu₂Si₂, which also move towards the Brillouin zone center upon cooling. These observations can be naturally understood now we have shown that magnetic excitations in CeCu₂Si₂ arise from heavy quasiparticles, and result from a combination of the intrinsic asymmetry of the magnetic dispersion and depletion of the electronic density of states near the Fermi level upon cooling (see Supplementary Note 2 and Supplementary Fig. 3 for details). Such a depletion occurs in A-type CeCu₂Si₂ due to a spin-density-wave gap, and in S-type CeCu₂Si₂ due to a superconducting gap.
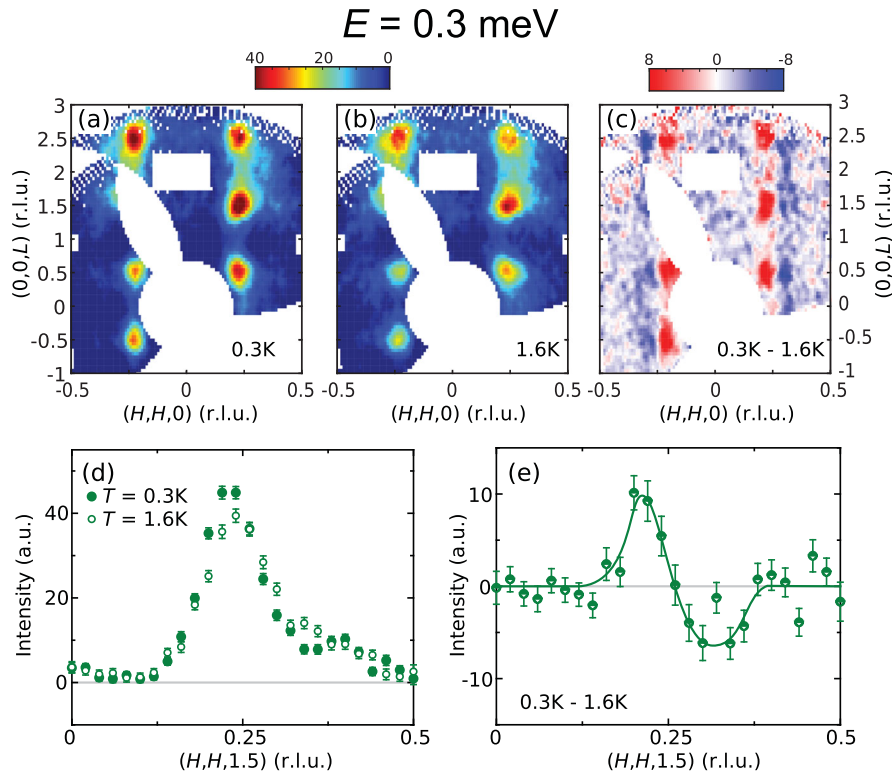
E = 0.3 meV

Fig. 4 Temperature dependence of the $E = 0.3$ meV magnetic excitations across T_c. $E = 0.3$ meV constant-energy maps of the $[H, H, L]$ plane for **a** $T = 0.3$ K, **b** $T = 1.6$ K, and **c** their difference. **d** Cuts along $(H, H, 1.5)$ from maps in (**a**) and (**b**), obtained by binning data with $1.4 < L < 1.6$. **e** The difference of cuts in (**d**). Data in this figure were measured using $E_f = 3$ meV. All vertical error bars represent statistical errors of 1 s.d.

Table 1. The relationship between magnetic exchange and superconducting condensation energies in unconventional superconductors.[16–21]

	$YBa_2Cu_3O_{6.95}$	$CeCoIn_5$	$CeCu_2Si_2$	$Ba_{0.67}K_{0.33}Fe_2As_2$	$Fe_{1+\delta}Te_{1-x}Se_x$ ($x \approx 0.5$)	$NaFe_{0.9785}Co_{0.0215}As$
$\frac{\Delta E_{mag}}{\Delta E_{SC}}$	≈ 16	≈ 35	≈ 21	≈ 7	≈ 24	≈ 26

Published ratios of the reduction in magnetic exchange energy in the superconducting state ΔE_{mag} with the superconducting condensation energy ΔE_{sc}, for cuprate, iron-based, and heavy fermion unconventional superconductors.

DISCUSSION

Our experimental observation of magnetic excitations extending up to at least $E = 5.5$ meV in $CeCu_2Si_2$ demonstrates quasi-2D magnetic fluctuations with an energy scale much larger than the superconducting pairing energy to be a common feature in unconventional superconductors. As the bandwidth of magnetic excitations is captured by effective magnetic interactions, which in turn determine the saving of magnetic exchange energy in the superconducting state ΔE_{mag}, the high-energy magnetic excitations observed in our work suggest a ΔE_{mag} that is at least as large as previously reported[18]. The commonality of a much larger ΔE_{mag} compared to the superconducting condensation energy ΔE_{SC} [Table 1] and the presence of a spin resonance mode[2,23,24] across different families of unconventional superconductors, suggest a common pairing mechanism and favors a sign-changing superconducting order parameter such as $d + d$[44] or $s^{\pm}$[45,46] for $CeCu_2Si_2$, rather than s^{++}[47]. To conclusively distinguish between these scenarios, it is important to study the dispersion of the spin resonance mode in comparison with theoretical results under different pairing symmetries to test its spin-excitonic nature[60–62]. Our work presents a model that captures the normal state magnetic excitations of $CeCu_2Si_2$, and is consistent with magnetically driven superconductivity in $CeCu_2Si_2$.

Given that the magnetic excitations in A-type $CeCu_2Si_2$ and the superconducting and normal states of S-type $CeCu_2Si_2$ are similar for $E \gtrsim 0.4$ meV[35,37], we expect the observed high energy excitations in our S-type $CeCu_2Si_2$ to also be present in A-type $CeCu_2Si_2$, as well as compositions in between. In addition, columnar spin excitations near τ are also seen in $CeNi_2Ge_2$, although compared to $CeCu_2Si_2$ no low-energy dispersive features were reported[63]. Since $CeNi_2Ge_2$ is paramagnetic and relatively far away from an AF QCP, this suggests that compared to the low-energy dispersive excitations, the columnar excitations at high energies are more robust upon tuning away from the QCP. In both cuprate and iron-based superconductors, the quasi-2D high energy magnetic excitations remain robust when tuning towards the superconducting state, while the low-energy excitations may change dramatically. Therefore, the prevalence of robust high-energy magnetic excitations suggests short-range 2D magnetic correlations provide a backdrop from which unconventional superconductivity emerges, while low-energy AF fluctuations and electronic structure can range from strongly 2D to having significant 3D features and are more tunable. This is analogous to conventional superconductors, in which a large Debye cutoff energy provides a backdrop for potential high-temperature superconductivity.

METHODS

Sample preparation and inelastic neutron scattering measurements

Several rod-shaped S-type $CeCu_2Si_2$ single crystal samples were grown using a vertical optical heating floating zone method [Supplementary Fig. 4a][49]. To avoid Si excess which results in A-type $CeCu_2Si_2$, we used a high-pressure Ar atmosphere and a relatively small overheating of the floating zone beyond the melting temperature, which effectively reduces Cu evaporation. Using inductively coupled plasma atomic-emission spectroscopy, we determined the atomic percentage of our samples to be Ce:20.1(1)%, Cu:40.3(1)%, and Si:39.6(1)%. This stoichiometry is found to be consistent across several pieces of our samples, indicating they are dominantly S-type[64], in agreement with previous transport measurements[49]. Specific heat measurements were carried out for several pieces of our $CeCu_2Si_2$ samples [Supplementary Fig. 4c], all exhibiting a specific heat jump below $T_c \approx 0.5$ K, different from A-type and A/S-type $CeCu_2Si_2$ samples[36,65]. The magnitude of the specific heat jump exhibits some sample dependence, possibly due to parts of the samples being nonsuperconducting. The specific heat measurements evidence our $CeCu_2Si_2$ samples are dominantly S-type, without prominent signatures of antiferromagnetism. While the presence of a minority phase of A-type or A/S-type $CeCu_2Si_2$ is difficult to rule out, the high-energy magnetic excitations uncovered in our work should also be present in A-type and A/S-type $CeCu_2Si_2$, as discussed above. Therefore, the possible presence of such minority phases will not affect the conclusions of our work.

We cut the rod-like samples into segments of a few centimeters and used the E3 four-circle neutron diffractometer to identify single-grain pieces by mapping the ϕ and χ rotation angles, with the scattering angle 2θ adjusted to the scattering angle of an intense structural Bragg peak. We then co-aligned four such segments in the $[H, H, L]$ plane, as shown in Supplementary Fig. 4b.

Inelastic neutron scattering measurements were carried out using the MACS[50] at the NIST center for neutron research in Gaithersburg, MD. Our measurements were carried out using fixed $E_f = 3$ or 5 meV, with Be filters placed after the sample for both E_f and before the sample for $E_f = 3$ meV. MACS consists of 20 spectroscopic detectors, and by rotating the sample and shifting the detectors, a map of the scattering plane at a fixed energy transfer can be efficiently constructed. The double-bounce analyzers are vertically focused, while the monochromator is doubly focused. Instrumental energy resolutions at the elastic line are $\Delta E \approx 0.14$ meV for $E_f = 3$ meV, and $\Delta E \approx 0.35$ meV for $E_f = 5$ meV. Sample alignment is confirmed on MACS for the (110) and (002) structural Bragg peaks. As shown in Supplementary Fig. 5, our samples are reasonably well-aligned for sample arrays used in inelastic neutron scattering measurements.

Extraction of experimental and calculated dispersions

To extract the experimental dispersion of magnetic excitations in $CeCu_2Si_2$, cuts along $(H, H, 1.48)$ were obtained by binning data with $1.38 < L < 1.58$ and fit using two Gaussian peaks

$$I(x) = a_1 \exp\left(-\frac{(x-\delta)^2}{2c^2}\right) + a_2 \exp\left(-\frac{(x-1+\delta)^2}{2c^2}\right). \quad (1)$$

The same expression with an additional constant term is used to extract the calculated dispersion. In these fittings, $x = 0$ corresponds to $(0, 0)$, $x = 1$ corresponds to $(1, 1)$ and δ is the fit peak center position. Representative fits to our experimental data are shown in the middle column of Fig. 3, and representative fits to our theoretical results are shown in Supplementary Fig. 6.

LDA+U band structure

The LDA+U band structure calculations were performed using the full-potential augmented plane-wave plus local orbital method as implemented in WIEN2k[66]. The Perdew–Burke–Ernzerhof exchange-correlation energy[67] was used with spin-orbit coupling and an effective on-site Coulomb interaction $U = 5$ eV[68]. The orbital characters were obtained using WANNIER90 code[69] via WIEN2WANNIER interface[70]. Our LDA+U band structure was used previously to study the pairing symmetry of $CeCu_2Si_2$[46], and is similar to band structures in previous LDA+U calculations[40,45] and from the renormalized band approach[71]. As the f-electrons are itinerant in our LDA+U calculations, the obtained Fermi surfaces are "large".

We note that there is a subtle difference in the band structures of refs. [45] and [46], with the latter used in the calculations of this work. Comparing the heavy electron Fermi surfaces in these two works, there is an extra ring-like Fermi surface in ref. [46] around the Γ point (Supplementary Fig. 7). This difference results from details in implementing the calculations, and affects neither key features of the band structure nor the expected physics, which is dominated by the cylindrical heavy electron Fermi surface common to refs. [45] and [46].

The partial density of states of $CeCu_2Si_2$ from our LDA+U calculations is shown in Supplementary Fig. 2. As can be seen, the Ce-$f_{5/2}$ density of states is mainly located just above the Fermi level, and decreases rapidly above 50 meV, becoming increasingly small around 100 meV. Such an evolution of the partial density of states is consistent with the notion that a change of character of the band states causes the crossover from dispersive to columnar magnetic excitations. However, as the partial density of states contains contributions from all the electronic states, and not just the well-nested regions that give rise to the magnetic excitations, the signatures for such a change is not as clear in the partial density of states compared to Fig. 3d.

Calculation of magnetic excitations in $CeCu_2Si_2$

The bare magnetic susceptibility with four indices is:

$$[\chi_0]_{\nu\nu'}^{\mu\mu'}(\mathbf{q}, i\omega_n) = -\sum_{\mathbf{k}, n_1, n_2} a_{n_1}^{\nu}(\mathbf{k}) a_{n_1}^{\nu'*}(\mathbf{k}) a_{n_2}^{\mu'}(\mathbf{k}+\mathbf{q}) a_{n_2}^{\mu*}(\mathbf{k}+\mathbf{q}) \quad (2)$$

$$\times \frac{1}{\beta} \sum_{i\omega_m} \frac{1}{i\omega_m - \epsilon_{n_1}(\mathbf{k})} \frac{1}{i\omega_m - i\omega_n - \epsilon_{n_2}(\mathbf{k}+\mathbf{q})} \quad (3)$$

where $a_n^{\mu}(\mathbf{k})$, $\epsilon_n(\mathbf{k})$ are the unitary matrices diagonalizing H_0 and the energy dispersion, respectively. The sum over n is taken over the entire band index. Using the Matsubara frequency sum rule and the Fermi-Dirac function $n_F(\epsilon) = \frac{1}{e^{\beta\epsilon}+1}$, we get:

$$[\chi_0]_{\nu\nu'}^{\mu\mu'}(\mathbf{q}, i\omega_n) = -\sum_{\mathbf{k}, n_1, n_2} a_{n_1}^{\nu}(\mathbf{k}) a_{n_1}^{\nu'*}(\mathbf{k}) a_{n_2}^{\mu'}(\mathbf{k}+\mathbf{q}) a_{n_2}^{\mu*}(\mathbf{k}+\mathbf{q})$$
$$\times \frac{n_F[\epsilon_{n_2}(\mathbf{k}+\mathbf{q})] - n_F[\epsilon_{n_1}(\mathbf{k})]}{i\omega_n + \epsilon_{n_2}(\mathbf{k}+\mathbf{q}) - \epsilon_{n_1}(\mathbf{k})} \quad (4)$$

using $i\omega \to \omega + i\eta$, we have

$$[\chi_0]_{\nu\nu'}^{\mu\mu'}(\mathbf{q}, \omega) = -\sum_{\mathbf{k}, n_1, n_2} a_{n_1}^{\nu}(\mathbf{k}) a_{n_1}^{\nu'*}(\mathbf{k}) a_{n_2}^{\mu'}(\mathbf{k}+\mathbf{q}) a_{n_2}^{\mu*}(\mathbf{k}+\mathbf{q})$$
$$\times \frac{n_F[\epsilon_{n_2}(\mathbf{k}+\mathbf{q})] - n_F[\epsilon_{n_1}(\mathbf{k})]}{\omega + \epsilon_{n_2}(\mathbf{k}+\mathbf{q}) - \epsilon_{n_1}(\mathbf{k}) + i\eta} \quad (5)$$

The transverse RPA susceptibility for a multiband system is:

$$\hat{\chi}_{RPA} = \frac{\hat{\chi}_0}{1 - \hat{U}\hat{\chi}_0} \quad (6)$$

This is in fact a Bethe-Salpeter equation where $\hat{U}$ is a $n^2 \times n^2$ matrix with orbital number n.

$$\hat{U}_{rr}^{rr} = U, \quad \hat{U}_{ss}^{rr} = U', \quad \hat{U}_{rs}^{rs} = J, \quad \hat{U}_{sr}^{rs} = J' \quad (r \neq s). \quad (7)$$

On-site interactions $U = U' = 0.25$ eV, $J = J' = 0$ eV, and a $20 \times 20 \times 20$ k-mesh were used in our RPA calculations, similar to previous work[45]. The U values used in our RPA calculations are smaller than those in our LDA+U calculations to avoid the divergence of RPA magnetic susceptibility. The key features of the RPA susceptibility are mostly determined by the bare susceptibility χ_0 (Supplementary Fig. 8), which already contains the essential features of the magnetic susceptibility, and are not strongly affected by the interaction term U.

Disclaimer: The identification of any commercial product or trade name does not imply endorsement or recommendation by the National Institute of Standards and Technology.

DATA AVAILABILITY

The data that support the findings of this study are available from the corresponding authors upon reasonable request.

CODE AVAILABILITY

The computer codes used for the LDA+U band structure calculations in this study are available from the corresponding authors upon reasonable request.

REFERENCES

1. Steglich, F. et al. Superconductivity in the presence of strong Pauli paramagnetism: $CeCu_2 Si_2$. *Phys. Rev. Lett.* **43**, 1892–1986 (1979).
2. Scalapino, D. J. A common thread: the pairing interaction for unconventional superconductors. *Rev. Mod. Phys.* **84**, 1383–1417 (2012).
3. Stewart, G. R. Unconventional superconductivity. *Adv. Phys.* **66**, 75–196 (2017).
4. Lee, P. A., Nagaosa, N. & Wen, X. G. Doping a Mott insulator: physics of high-temperature superconductivity. *Rev. Mod. Phys.* **78**, 17–84 (2006).
5. Keimer, B., Kivelson, S. A., Norman, M. R., Uchida, S. & Zaanen, J. From quantum matter to high-temperature superconductivity in copper oxides. *Nature* **518**, 179–186 (2015).
6. Sidis, Y. et al. Inelastic neutron scattering study of spin excitations in the superconducting state of high temperature superconductors. *Comptes Rendus Phys.* **8**, 745–762 (2007).
7. Stewart, G. R. Superconductivity in iron compounds. *Rev. Mod. Phys.* **83**, 1589–1652 (2011).
8. Dai, P. C. Antiferromagnetic order and spin dynamics in iron-based superconductors. *Rev. Mod. Phys.* **87**, 855–896 (2015).
9. Fernandes, R. M., Chubukov, A. V. & Schmalian, J. What drives nematic order in iron-based superconductors? *Nat. Phys.* **10**, 97–104 (2014).
10. Si, Q., Yu, R. & Abrahams, E. High-temperature superconductivity in iron pnictides and chalcogenides. *Nat. Rev. Mater.* **1**, 16017 (2016).
11. Pfleiderer, C. Superconducting phases of f-electron compounds. *Rev. Mod. Phys.* **81**, 1551–1624 (2009).
12. Stockert, O., Kirchner, S., Steglich, F. & Si, Q. Superconductivity in Ce- and U-Based 122 heavy-fermion compounds. *J. Phys. Soc. Jpn.* **81**, 011001 (2012).
13. White, B. D., Thompson, J. D. & Maple, M. B. Unconventional superconductivity in heavy-fermion compounds. *Phys. C.* **514**, 246–278 (2015).
14. Moriya, T. & Ueda, K. Antiferromagnetic spin fluctuation and superconductivity. *Rep. Prog. Phys.* **66**, 1299–1341 (2003).
15. Demler, E. & Zhang, S. C. Quantitative test of a microscopic mechanism of high-temperature superconductivity. *Nature* **396**, 733–735 (1998).
16. Woo, H. et al. Magnetic energy change available to superconducting condensation in optimally doped $YBa_2 Cu_3 O_{6.95}$. *Nat. Phys.* **2**, 600–604 (2006).
17. Stock, C., Broholm, C., Hudis, J., Kang, H. J. & Petrovic, C. Spin resonance in the d-wave superconductor $CeCoIn_5$. *Phys. Rev. Lett.* **100**, 087001 (2008).
18. Stockert, O. et al. Magnetically driven superconductivity in $CeCu_2 Si_2$. *Nat. Phys.* **7**, 119–124 (2011).
19. Wang, M. et al. Doping dependence of spin excitations and its correlations with high-temperature superconductivity in iron pnictides. *Nat. Commun.* **4**, 2874 (2013).
20. Leiner, J. et al. Modified magnetism within the coherence volume of superconducting $Fe_{1+\delta} Se_x Te_{1-x}$. *Phys. Rev. B* **90**, 100501(R) (2014).
21. Carr, S. V. et al. Electron doping evolution of the magnetic excitations in $NaFe_{1-x} Co_x As$. *Phys. Rev. B* **93**, 214506 (2016).
22. Dahm, T. et al. Strength of the spin-fluctuation-mediated pairing interaction in a high-temperature superconductor. *Nat. Phys.* **5**, 217–221 (2009).
23. Eschrig, E. The effect of collective spin-1 excitations on electronic spectra in high-T_c superconductors. *Adv. Phys.* **55**, 47–183 (2006).
24. Yu, G., Li, Y., Motoyama, E. M. & Greven, M. A universal relationship between magnetic resonance and superconducting gap in unconventional superconductors. *Nat. Phys.* **5**, 873 (2009).
25. Waßer, F. et al. Strong spin resonance mode associated with suppression of soft magnetic ordering in hole-doped $Ba_{1-x} Na_x Fe_2 As_2$. *npj Quantum Mater.* **4**, 59 (2019).
26. Birgeneau, R. J., Stock, C., Tranquada, J. M. & Yamada, K. Magnetic neutron scattering in hole-doped cuprate superconductors. *J. Phys. Soc. Jpn.* **75**, 111003 (2006).
27. Lipscombe, O. J., Hayden, S. M., Vignolle, B., McMorrow, D. F. & Perring, T. G. Persistence of high-frequency spin fluctuations in overdoped superconducting $La_{2-x} Sr_x CuO_4$ ($x = 0.22$). *Phys. Rev. Lett.* **99**, 067002 (2007).
28. Fujita, M. et al. Progress in neutron scattering studies of spin excitations in high-T_c cuprates. *J. Phys. Soc. Jpn.* **81**, 011007 (2012).
29. Le Tacon, M. et al. Intense paramagnon excitations in a large family of high-temperature superconductors. *Nat. Phys.* **7**, 725–730 (2011).
30. Le Tacon, M. et al. Dispersive spin excitations in highly overdoped cuprates revealed by resonant inelastic x-ray scattering. *Phys. Rev. B* **88**, 020501(R) (2013).
31. Dean, M. P. M. et al. Persistence of magnetic excitations in $La_{2-x} Sr_x CuO_4$ from the undoped insulator to the heavily overdoped non-superconducting metal. *Nat. Mater.* **12**, 1019–1023 (2013).
32. Liu, M. et al. Nature of magnetic excitations in superconducting $BaFe_{1.9} Ni_{0.1} As_2$. *Nat. Phys.* **8**, 376–381 (2012).
33. Zhou, K. J. et al. Persistent high-energy spin excitations in iron-pnictide superconductors. *Nat. Commun.* **4**, 1470 (2013).
34. Gegenwart, P. et al. Breakup of heavy fermions on the brink of phase A in $CeCu_2 Si_2$. *Phys. Rev. Lett.* **81**, 1501 (1998).
35. Arndt, J. et al. Spin fluctuations in normal state $CeCu_2 Si_2$ on approaching the quantum critical point. *Phys. Rev. Lett.* **106**, 246401 (2011).
36. Stockert, O. et al. Nature of the a phase in $CeCu_2 Si_2$. *Phys. Rev. Lett.* **92**, 136401 (2004).
37. Huesges, Z. et al. Robustness of magnons near the quantum critical point in the heavy-fermion superconductor $CeCu_2 Si_2$. *Phys. Rev. B* **98**, 134425 (2018).
38. Eremin, I., Zwicknagl, G., Thalmeier, P. & Fulde, P. Feedback spin rsonance in superconducting $CeCu_2 Si_2$ and $CeCoIn_5$. *Phys. Rev. Lett.* **101**, 187001 (2008).
39. Akbari, A. & Thalmeier, P. Spin excitations in the fully gapped hybridized two band superconductor. *Annals of Physics* **428**, 168433 (2021).
40. Kittaka, S. et al. Multiband superconductivity with unexpected deficiency of nodal quasiparticles in $CeCu_2 Si_2$. *Phys. Rev. Lett.* **112**, 067002 (2014).
41. Yamashita, T. et al. Fully gapped superconductivity with no sign change in the prototypical heavy-fermion $CeCu_2 Si_2$. *Sci. Adv.* **3**, e1601667 (2017).
42. Takenaka, T. et al. Full-gap superconductivity robust against disorder in heavy-fermion $CeCu_2 Si_2$. *Phys. Rev. Lett.* **119**, 077001 (2017).
43. Kittaka, S. et al. Thermodynamic study of gap structure and pair-breaking effect by magnetic field in the heavy-fermion superconductor $CeCu_2 Si_2$. *Phys. Rev. B* **94**, 054514 (2016).
44. Pang, G. et al. Fully gapped d-wave superconductivity in $CeCu_2 Si_2$. *Proc. Natl Acad. Sci. U.S.A.* **115**, 5343–5347 (2017).
45. Ikeda, H., Suzuki, M. T. & Arita, R. Emergent loop-nodal $s^\pm$-wave superconductivity in $CeCu_2 Si_2$: similarities to the iron-based superconductors. *Phys. Rev. Lett.* **114**, 147003 (2015).
46. Li, Y. et al. Gap symmetry of the heavy-fermion superconductor $CeCu_2 Si_2$ at ambient pressure. *Phys. Rev. Lett.* **120**, 217001 (2018).
47. Tazai, R. & Kontani, H. Fully gapped s-wave superconductivity enhanced by magnetic criticality in heavy-fermion systems. *Phys. Rev. B* **98**, 205107 (2018).
48. Tazai, R. & Kontani, H. Hexadecapole fluctuation mechanism for s-wave heavy fermion superconductor $CeCu_2 Si_2$: interplay between intra- and inter-orbital cooper pairs. *J. Phys. Soc. Jpn.* **88**, 063701 (2019).
49. Cao, C. D. et al. Single crystal growth of the $CeCu_2 Si_2$ intermetallic compound by a vertical floating zone method. *Cryst. Growth Des.* **11**, 431–435 (2011).
50. Rodriguez, J. A. et al. Measurement science and technology MACSa new high intensity cold neutron spectrometer at NIST. *Meas. Sci. Technol.* **19**, 034023 (2008).
51. Horigane, K. et al. Spin excitations in hole-overdoped iron-based superconductors. *Sci. Rep.* **6**, 33303 (2016).
52. Tomiyoshi, S., Yamaguchi, Y., Ohashi, M., Cowley, E. R. & Shirane, G. Magnetic excitations in the itinerant antiferromagnets $Mn_3 Si$ and Fe-doped $Mn_3 Si$. *Phys. Rev. B* **36**, 2181–2189 (1987).
53. Chen, X. et al. Unconventional Hund metal in a weak itinerant ferromagnet. *Nat. Commun.* **11**, 3076 (2020).
54. de' Medici, L., Giovannetti, G. & Capone, M. Selective Mott physics as a key to iron superconductors. *Phys. Rev. Lett.* **112**, 177001 (2014).
55. Yi, M., Zhang, Y., Shen, Z. X. & Lu, D. Role of the orbital degree of freedom in iron-based superconductors. *npj Quant. Mater.* **2**, 57 (2017).
56. Zhang, C. et al. Effect of pnictogen height on spin waves in iron pnictides. *Phys. Rev. Lett.* **112**, 217202 (2014).
57. Goremychkin, E. A. et al. Coherent band excitations in $CePd_3$: a comparison of neutron scattering and ab initio theory. *Science* **359**, 186–191 (2018).
58. Butch, N. P. et al. Symmetry and correlations underlying hidden order in $URu_2 Si_2$. *Phys. Rev. B* **91**, 035128 (2015).
59. Portnichenko, P. Y., Cameron, A. S. & Inosov, D. S., Neutron-Scattering Studies of Spin Dynamics in Pure and Doped CeB_6 ", Rare Earth Borides, edited by D. S. Inosov, Jenny Stanford Publishing (2021).
60. Song, Y. et al. Robust upward dispersion of the neutron spin resonance in the heavy fermion superconductor $Ce_{1-x} Yb_x CoIn_5$. *Nat. Commun.* **7**, 12774 (2016).
61. Song, Y. et al. Nature of the spin resonance mode in $CeCoIn_5$. *Commun. Phys.* **3**, 98 (2020).
62. Hong, W. et al. Neutron spin resonance in a quasi-two-dimensional iron-based superconductor. *Phys. Rev. Lett.* **125**, 117002 (2020).
63. Fåk, B., Flouquet, J., Lapertot, G., Fukuhara, T. & Kadowaki, H. Magnetic correlations in single-crystalline $CeNi_2 Ge_2$. *J. Phys.: Condens. Matter* **12**, 5423–5435 (2000).

64. Steglich, F. et al. New observations concerning magnetism and superconductivity in heavy-fermion metals. *Physica B* **223–224**, 1–8 (1996).

65. Lengyel, E., Nicklas, M., Jeevan, H. S., Geibel, C. & Steglich, F. Pressure tuning of the interplay of magnetism and superconductivity in $CeCu_2 Si_2$. *Phys. Rev. Lett.* **107**, 057001 (2011).

66. Blaha, P., Schwarz, K., Madsen, G. K. H., Kvasnicka, D. & Luitz, J., *WIEN2k: An Augmented Plane Wave + Local Orbitals Program for Calculating Crystal Properties* (Karlheinz Schwarz, Technische Universität Wien, 2014).

67. Perdew, J. P., Burke, K. & Ernzerhof, M. Generalized gradient approximation made simple. *Phys. Rev. Lett.* **77**, 3865–3868 (1996).

68. Anisimov, V. I., Aryasetiawa, F. & Lichtenstein, A. I. First-principles calculations of the electronic structure and spectra of strongly correlated systems: the LDA+ U method. *J. Phys.: Condens. Matter* **9**, 767–808 (1997).

69. Mostofi, A. A. et al. wannier90: a tool for obtaining maximally-localised Wannier functions. *Comput. Phys. Commun.* **178**, 685–699 (2008).

70. Kuneš, J. et al. Wien2wannier: from linearized augmented plane waves to maximally localized Wannier functions. *Comput. Phys. Commun.* **181**, 1888–1895 (2010).

71. Zwicknagl, G. & Pulst, W. $CeCu_2 Si_2$: renormalized band structure, quasiparticles and co-operative phenomena. *Physica B* **186–188**, 895–898 (1993).

ACKNOWLEDGEMENTS

AUTHOR CONTRIBUTIONS

P.D., Y.Song, and C.C. conceived the project. C.C. and W.L. prepared the samples. Z.Y. and Y.Song co-aligned the samples. W.W., Y.Song, C.C., and Y.Q. carried out the experiments. W.W. and Y.Song analyzed the data. Y.X., Y.Sheng, and Y.Y. carried out the theoretical analyses. Y.Song, P.D., and Y.Y. wrote the paper with input from all authors.

COMPETING INTERESTS

The authors declare no competing interests.

ADDITIONAL INFORMATION

Supplementary information The online version contains supplementary material available at https://doi.org/10.1038/s41535-021-00358-x.

Correspondence and requests for materials should be addressed to Y.S., C.C. or P.D.

Reprints and permission information is available at http://www.nature.com/reprints

Publisher's note Springer Nature remains neutral with regard to jurisdictional claims in published maps and institutional affiliations.